



Hybrid catalysts for the selective catalytic reduction (SCR) of NO by NH₃: Precipitates and physical mixtures

Mariam Salazar^{a,1}, Stefanie Hoffmann^b, Lukas Tillmann^a, Vera Singer^a, Ralf Becker^c, Wolfgang Grünert^{a,*}

^a Lehrstuhl für Technische Chemie, Ruhr-Universität Bochum, D-44780 Bochum, Germany

^b Inorganic Chemistry, University Duisburg-Essen, Campus Essen, Essen, Germany

^c Huntsman P&A Germany, 47198 Duisburg, Germany



ARTICLE INFO

Article history:

Received 6 April 2017

Received in revised form 23 June 2017

Accepted 26 June 2017

Available online 28 June 2017

Keywords:

NH₃-SCR

Hybrid catalysts

Physical mixture

Precipitate

ABSTRACT

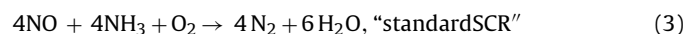
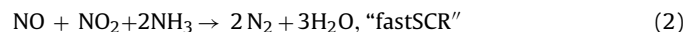
Hybrid catalysts for the selective catalytic reduction of NO by NH₃, which have been introduced as physical mixtures between an oxidation catalyst and an SCR catalyst, have been prepared by precipitation of the former onto the latter. Mn oxide, CeO₂, and CeZrO_x have been employed as oxidation components, Fe-ZSM-5 and H-ZSM-5 as SCR components (acidic components). The catalysts have been characterized by XRD, nitrogen physisorption and temperature-programmed reduction after thermal treatments at 623 K or at 923 K, their catalytic behavior has been examined by standard techniques. In the Ce-containing systems, precipitated hybrids were more active than physically mixed hybrids. A reversed ranking in the case of the MnO_x/Fe-ZSM-5 system may be due to a particular susceptibility of the corresponding precipitates to deactivation. A lack of correlation between BET surface areas, which indicate accessibility of the zeolite interior, and activity suggests that the reaction does not utilize the whole zeolite crystal. Precipitated hybrids were very prone to thermal deactivation, in particular those containing MnO_x or CeO₂. This was ascribed to an increased opportunity for the redox oxides to undergo solid-state ion exchange when deposited onto the zeolite crystals. When the extent of deactivation was more drastic, it was accompanied by a significant decrease of the apparent activation energy of NH₃-SCR. This may support earlier conclusions according to which the reaction mechanism operating in the hybrids comprises a transport step of an unstable intermediate, which might become rate limiting when acidic sites in the vicinity of the oxidation sites are poisoned by solid-state ion exchange.

© 2017 Elsevier B.V. All rights reserved.

1. Introduction

The selective catalytic reduction (SCR) of nitrogen oxides remains a key topic in environmental catalysis. While commercialized both for stationary and mobile sources, the technology may benefit from development of catalysts with improved low-temperature behavior [1,2]. Pronounced synergistic effects occurring in physical mixtures of oxidation and SCR catalysts, which were first reported by Stakheev et al. [3–6] may become productive in this search. The synergies in these combined catalysts (or hybrid catalysts) were originally ascribed to a mechanism in which the oxidation component produces NO₂ (Eq. (1)). This enables the

SCR component to operate via fast SCR (2), which would result in an accelerated conversion according to the stoichiometry of standard SCR (3).



Our recent work on these catalysts [7–9], in which various SCR components (Fe-ZSM-5, H-ZSM-5, V₂O₅-WO₃/TiO₂) were combined with a number of oxidation catalysts, has raised, however, doubt about this simple scheme. The synergistic effect was observed to depend strongly on the distance between components, which implies that the species transferring the reaction from one component to the other one is unstable [8]. Comparing reaction rates of fast SCR over the SCR component and standard SCR over hybrids made of this very component, we found conditions where the latter reaction (standard SCR) was faster than the former. Fast SCR

* Corresponding author at: Lehrstuhl für Technische Chemie, Ruhr-Universität Bochum, P. O. Box 102148, D-44780 Bochum, Germany.

E-mail address: w.gruenert@techem.rub.de (W. Grünert).

¹ Present address: Technip, E. Weymouth, Massachusetts-02189, U.S.A.

should therefore not be part of the reaction mechanism of standard SCR over the hybrids [7]. Operating with a transport step of an unstable intermediate, the hybrid catalysts are reminiscent of a system described by us earlier, in which CeO_2 and H-ZSM-5 were combined in physical mixtures or precipitates. These exhibited attractive activities in the SCR of NO by methane [10,11] although none of the components were good for this reaction when applied separately, while Ce-exchanged zeolites operate only with higher hydrocarbons [12].

The short life time of critical intermediates interferes with their easy identification, but it suggests on the other hand that performance of the hybrids may be improved by further decreasing the distance between the components. As exemplified earlier with the $\text{CeO}_2/\text{H-ZSM-5}$ system for CH_4 -SCR [10,11], this may be achieved by precipitating the oxidation component on the external zeolite surface. While active sites on this surface may be blocked, plenty of sites will remain to be available in the zeolite cavities. The present paper reports on an effort to examine the potential of this approach for the preparation of hybrid catalysts for NH_3 -SCR.

2. Experimental

2.1. Catalysts

SCR components employed were H-ZSM-5 and Fe-ZSM-5 in two batches, the Fe content of which was 0.4 and 0.5 wt-% as determined by ICP-OES. Fe-ZSM-5 was made from a NH_4 -ZSM-5 ($\text{Si}/\text{Al} \approx 14$) donated by Tricat Zeolites Bitterfeld (now a Clariant company). Fe was introduced into the H form obtained by calcination of the NH_4 form at 773 K by solid-state ion exchange (SSIE) as described in detail by Schwidder et al. [13]. The zeolite was ground with a given amount of $\text{FeCl}_3 \cdot 6\text{H}_2\text{O}$, the mixture was heated in inert gas at 573 K for 1 h, the product was washed, dried, and calcined in synthetic air (20% O_2 in He) at 873 K for 2 h.

Oxidation components employed were based on CeO_2 , Ce-Zr mixed oxide, and manganese oxide. The binary oxides were made by precipitation of the hydroxides from 0.5 M aqueous solutions of Mn(II) and Ce(III) nitrate with ammonia solution (25%, until $\text{pH} = 8$). The precipitates were aged at room temperature for 1 h, washed, dried, and calcined in air at 623 K or at 923 K. Yields of this preparation were very different: 62% for CeO_2 , but only 18% for Mn_2O_3 . The same procedure was employed to precipitate the oxides onto the external surface of Fe-ZSM-5, with intended weight ratios of oxide/zeolite of 1 and 1/3. Here as well, calcination was performed at 623 K or at 923 K.

CeZrO_x was precipitated from a 1 M (in total) solution of $\text{Ce}(\text{NO}_3)_3$ and $\text{ZrO}(\text{NO}_3)_2$ at a Ce: Zr ratio of 7/3 with dilute NH_3 (1.2 M) at $\text{pH} = 8.5$. The precipitate was aged, washed, dried, and calcined at 623 K or 923 K. This material will be labeled as $\text{CeZr}(\text{Bo})$, because for some purposes, a commercial ceria-zirconia mixed oxide donated by Umicore & Co. KG was employed. The latter will be designated as $\text{CeZr}(\text{U})$. CeZrO_x was also precipitated onto H-ZSM-5 or onto Fe-ZSM-5 (with 0.4 wt-% Fe; oxide-zeolite ratios – 1 and 1/3) by suspending the zeolites in the above-mentioned solution of the nitrates and precipitating with dilute ammonia solution. The precipitates were calcined at 623 K or 923 K.

For the catalytic studies, the powders were pressed, crushed, and sieved to obtain an appropriate particle size (250–350 μm , 45–60 mesh).

These precipitated hybrid catalysts were compared with physical (or mechanical) mixtures containing both components at a 1:1 weight ratio. The corresponding mixture was thoroughly ground in a mortar before processing it into mixed particles as indicated above. The particles were subjected to calcinations at 623 K and 923 K.

2.2. Characterization

Sample compositions were analyzed by ICP-OES using a UNICAM PU 701 spectrometer. Samples were digested by peroxide fusion (Mn-based materials) or by lithium borate fusion (Ce-containing samples). Textural characterization was obtained from nitrogen adsorption-desorption isotherms measured at 77 K with a NOVA-2000 instrument (Quantachrome). Initially, samples were outgassed at 573 K under a residual pressure of 10^{-3} mbar for 3 h. Surface areas were evaluated from the BET model. Phase compositions of the catalysts were characterized by XRD measurements in reflection geometry with an Empyrean Theta-Theta diffractometer (Panalytical, Almelo) using a Cu anode ($\lambda = 1.54056 \text{ \AA}$). The K-beta emission line was suppressed by a Ni Filter. Samples were scanned in the 2–70° 2Θ range at ambient temperature.

Selected catalysts were also studied by temperature-programmed reduction (TPR), which was made by heating the samples in 4.5 vol-% H_2 up to 1123 K at 5 K/min, with a 1 h isothermal period at this temperature. The effluent gas was analyzed by a Hydros thermal conductivity detector (Fisher-Rosemount).

2.3. Catalytic measurements

Reaction rates of standard SCR were measured in flow regime (microflow quartz reactor, 4.2 mm i.d.) at atmospheric pressure and temperatures between 423 and 873 K. Gas lines after and before the reactors were kept at 350 K to avoid water condensation. The GHSV was 300,000 h^{-1} for the hybrid catalysts (catalyst mass – 25 mg) while 600,000 h^{-1} (catalyst mass – 12.5 mg) were employed for individual components in order to identify their possible contribution to the behavior of the hybrid systems. The feed consisted of 1000 ppm NO, 1000 ppm NH_3 , 2 vol-% O_2 , balanced with He. In the steady state, NO and NH_3 concentrations were determined online using an XStream X2 Gas Analyzer (Rosemount Analytical; Emerson) which combines non-dispersive infrared and ultraviolet spectrometry for quantitative analysis. The same instrument was used to check for NO_2 while N_2O formation was examined with an ABB Advanced Optima Continuous Gas Analyzer (A02000 Series). Conversions were calculated according to: $X_i (\%) = \frac{c_{i,\text{in}} - c_{i,\text{out}}}{c_{i,\text{in}}} \times 100\%$ ($i = \text{NO}$ or NH_3).

3. Results

3.1. Characterization

3.1.1. Composition

Compositions achieved in the precipitation preparations are given in Table 1 where the labels of the samples are presented as well. They consist of the targeted wt-% of oxide (denoted as "Mn", "Ce", or "CeZr") in the sample in parentheses, the kind of zeolite (Fe- or H-ZSM-5) and the temperature of calcination. Initial P or MM differentiates between precipitates and physical (mechanical) mixtures.

While the intended oxide/zeolite ratios were nearly achieved with Ce-based preparations, the Mn-based precipitates deviate strongly from the targeted values. This parallels the low yield in the preparation of Mn_2O_3 and seems to be due to a relatively high solubility of Mn^{2+} at the pH employed. However, important results were achieved also with these samples, while there was no indication that increased Mn content could improve the performance (see below). Precipitates with higher Mn content were therefore not prepared. In the mixed oxide catalysts, the targeted 70/30 atomic ratios between Ce and Zr was nicely met (see footnotes to Table 1), but the oxide content of the precipitates was somewhat smaller than intended.

Table 1
Chemical compositions and BET surface areas of catalysts.

Catalyst	wt-% Mn, Ce, Zr (as Mn_2O_3 , CeO_2 , CeZrO_x)	BET surface area ^a m^2/g
Mn(623)		26
Mn(923)		20.4
P(50)Mn/Fe-Z(623)	3.8 (5.4)	326
P(50)Mn/Fe-Z(923)		309
P(25)Mn/Fe-Z(623)	2.6 (3.8)	335
P(25)Mn/Fe-Z(923)		235
Ce(623)		66
Ce(923)		5
P(50)Ce/Fe-Z(623)	44.8 (55.0)	198
P(50)Ce/Fe-Z(923)		171
P(25)Ce/Fe-Z(623)	25.8 (31.7)	267
P(25)Ce/Fe-Z(923)		236
CeZr(623) ^b	Ce: 58.9; Zr: 15.1 ^c	126
CeZr(923) ^b		37
P(50)CeZr/H-Z(623)	Ce: 22.5; Zr: 6.5 ^d (36.9)	320
P(50)CeZr/H-Z(923)		233
P(25)CeZr/H-Z(623)	Ce: 12.0; Zr: 3.0 ^e (18.9)	314
P(25)CeZr/H-Z(923)		306
P(50)CeZr/Fe-Z(623)	Ce: 21.5; Zr: 6.1 ^f (34.7)	265
P(50)CeZr/Fe-Z(923)		222

^a Fe-ZSM-5-339 m^2/g .

^b CeZr(Bo).

^c Ce/Zr = 71.7/28.3.

^d Ce/Zr = 69.3/30.7.

^e Ce/Zr = 72.3/27.7.

^f Ce/Zr = 69.6/30.4.

3.1.2. XRD

X-ray diffractograms of the individual components and of MnO_x - and CeO_2 -based precipitated hybrids are compared in Fig. 1. It should be noted that the diffractograms are not all on the same intensity scale. As expected, no Fe-containing phases could be observed in Fe-ZSM-5. From the Mn oxide calcined at 623 K, only signals of Mn_3O_4 were obtained while Mn_2O_3 was formed after calcination at 923 K (Fig. 1a). In the precipitates with Fe-ZSM-5, Mn-containing phases could hardly be discerned. It is, however, difficult to tell to which extent this is due to its structural disorder or to the low Mn oxide concentration (Table 1). After calcination at 923 K, a signal at $2\Theta = 33^\circ$ (see arrows) was somewhat more pronounced and broader than the one present in the zeolite, which may indicate the formation of small Mn_2O_3 crystallites on the surface of the zeolite crystals.

CeO_2 crystals were detected in all ceria-containing samples (Fig. 1b). Crystal sizes estimated from the Scherrer equation, which are included in the figure, show the biggest particles after calcination of unsupported CeO_2 at 923 K. Its (primary) particle size after low-temperature calcination was just 18 nm. The zeolite signals appear strongly attenuated because the intensity scale is dominated here by the heavy scatterer Ce. Notably, calcination of the CeO_2 -based precipitates at 623 K resulted in a very similar particle size of 15 nm. After high-temperature calcination, the particles size grew bigger at the larger Ce content, to 45 and 23 nm for 50% and 25% CeO_2 , respectively.

Analogous data for CeZrOx precipitated with and without Fe-ZSM-5 or H-ZSM-5 are shown in Fig. 2. The broad signals of unsupported CeZr(Bo) after calcination at 623 K are centered between the positions of CeO_2 and ZrO_2 , though leaning more towards CeO_2 . After calcination at 923 K, narrower signals indicate increased particle sizes. In the diffractograms of the precipitates, the zeolite signals are better visible than in those of the $\text{CeO}_2/\text{Fe-ZSM-5}$ samples (cf. Fig. 1b) although the oxide contents are not much different. This is most likely caused by attenuated intensities of oxide reflections due to the presence of the lighter element Zr.

The more intense interference of oxide and zeolite signals prevents extracting the width of the oxide reflections. However, the lack of resolution between signals at $2\Theta \approx 29^\circ$ and 33.5° in P(25)CeZr/H-Z(623), and likewise in P(50)CeZr/Fe-Z(623) (Fig. 2b), which are well separated in the diffractogram of CeZr(Bo, 623), indicates a smaller particle size in the former materials. After calcination at 923 K, the diffractograms of the precipitates on Fe-Z (Fig. 2b) are very similar to those of P(50)CeZr/H-Z (Fig. 2a). The lines are clearly broader than those of CeO_2 in the analogous Ce-only catalysts (Fig. 1b).

3.1.3. Physical surface area

BET surface areas measured with our catalysts are collected in Table 1. It should be noted that accuracy of such measurements is limited with microporous materials like zeolites because of capillary condensation at low pressures, but relative trends can certainly be discussed. The unsupported oxides have external surface areas between 26 and 126 m^2/g , which decrease after high-temperature calcination. As expected, the decrease is more severe with CeO_2 than with the Ce-ZrOx mixed oxide.

Precipitating Mn oxide onto Fe-ZSM-5 did not affect the BET surface area of the zeolite significantly. Calcination at 923 K, however, decreased the surface area, in case of P(25)Mn/Fe-Z drastically. The smaller BET surface areas of the CeO_2 -based hybrids certainly indicates more extensive pore plugging due to the larger precipitate content. Calcination at 923 K decreased the surface area moderately, again more pronounced in the sample with the smaller precipitate content. With P(50)CeZr precipitated onto Fe-ZSM-5 or H-ZSM-5, similar BET surface areas were obtained only after high-temperature calcination while the values after low-temperature calcination were clearly larger, in particular for the sample containing H-ZSM-5. In P(25)CeZr/H-Z, the pore blocking effect was minor even after treatment at 923 K.

3.1.4. Temperature-programmed reduction

TPR measurements have been made to achieve additional evidence on the speciation of the oxidation component in the MnO_x - and CeO_2 -based hybrids. The data is summarized in Fig. 3 together with profiles of reference compounds.

The profile of Fe-ZSM-5 consists of a very small signal at 493 K hardly deviating from the baseline. The MnO_2 reference exhibited two peaks in agreement with literature, where these were assigned to reduction to Mn_3O_4 via Mn_2O_3 (low-temperature), and further to MnO (high-temperature) [14,15]. The profiles of P(50)Mn/Fe-Z include a signal in the same temperature region, which suggests the presence of bulk Mn oxide particles on the external zeolite surface. The higher reduction temperature required after calcination at 923 K may indicate a better ordering of the crystallites. In P(50)Mn/Fe-Z(623), there were also peaks below 573 K, which disappeared during high-temperature calcination. In both cases, the curve begins to gradually increase around 1000 K. A completely different TPR profile was obtained for P(25)Mn/Fe-Z calcined at 923 K. Although hydrogen consumption started already around 573 K, there was no peak in the profile: the signal increased to a certain level and remained there up to 1123 K.

Table 2 reports H_2 consumptions in the temperature range studied and compares them with expectations on the basis of an initial Mn(III) state as observed by XRD for the severely calcined unsupported oxide (Fig. 1a). Evaluation of consumption is difficult with the rather small signals because of possible baseline drifts. We used the behavior in the isothermal period at 1123 K (not shown) to check this option: if the signal results from real H_2 consumption it will gradually decay in this period. As this was not the case for the Mn-containing samples, the signal was alternatively integrated in narrower limits for P(50)Mn/Fe-Z (see arrows in Fig. 3a) or on an inclined baseline for P(25)Mn/Fe-Z(623). These results are

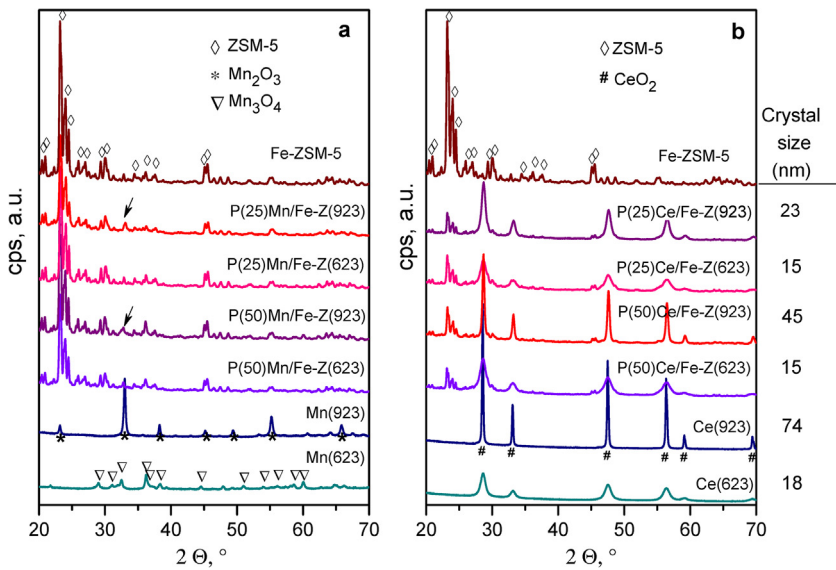


Fig. 1. X-ray diffractograms of precipitated hybrid catalysts and of pure compounds after calcination at 623 K or 923 K, a – MnO_x-based catalysts, b – CeO₂-based catalysts, with CeO₂ particle sizes estimated from Scherrer equation. Diffractograms may be on different cps scales.

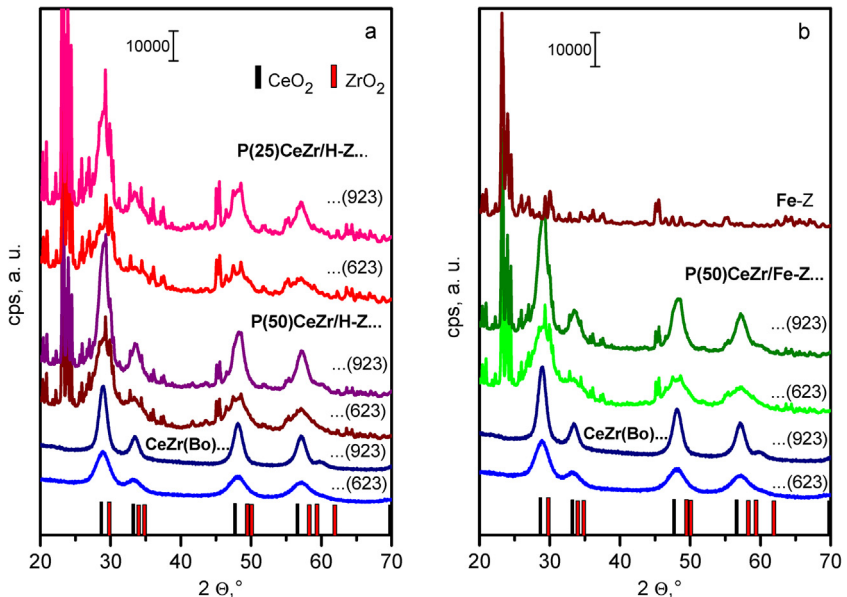


Fig. 2. X-ray diffractograms of precipitated hybrid catalysts and of pure compounds after calcination at 623 K or 923 K, systems with CeZrO_x mixed oxide, a – precipitates onto H-ZSM-5, b – precipitate onto Fe-ZSM-5. Diffractograms may be on different cps scales.

Table 2
Reduction conversions during TPR measurements (cf. Fig. 3).

Catalyst	Mn ³⁺ → Mn ²⁺ Ce ⁴⁺ → Ce ³⁺ expected, mmol/g	Mn ³⁺ → Mn ²⁺ Ce ⁴⁺ → Ce ³⁺ measured, mmol/g
P(50)Mn/Fe-Z(623)	0.34	0.48 (0.71 ^a)
P(50)Mn/Fe-Z(923)	0.34	0.17 (0.33 ^a)
P(25)Mn/Fe-Z(923)	0.24	0.06 (0.24 ^a)
P(50)Ce/Fe-Z(623)	1.68	0.74
P(50)Ce/Fe-Z(923)	1.68	0.67
P(25)Ce/Fe-Z(923)	0.92	0.41

^a full range, without baseline correction.

given in Table 2 as well. Irrespective of the baseline selected, a high hydrogen consumption indicates the presence of Mn species in oxidation states >3 in P(50)Mn/Fe-Z calcined at 623 K, which may

have caused the low-temperature consumption peaks. After high-temperature calcination, H₂ consumption decreased significantly and indicated that most likely some of the Mn became irreducible, in P(25)Mn/Fe-Z(923) more than in P(50)Mn/Fe-Z(923). As bulk Mn(III) oxide phases are easily reduced below 1000 K, this strongly suggests interactions with the zeolite (SSIE, or reaction to silicate phases). While destruction of the zeolite is not supported by the diffractograms (Fig. 1a), the changes are more likely caused by SSIE (see below).

TPR profiles of CeO₂/Fe-ZSM-5 composites are shown in Fig. 3b. Again, high calcination temperatures caused major changes in the curves. CeO₂ is known to exhibit two TPR signals, with a low-temperature peak arising from Ce⁴⁺ → Ce³⁺ reduction in the surface layer while progression of the reduction into the bulk occurs at higher temperatures [16,17]. In P(50)Ce/Fe-Z(623), an intense low-temperature signal with several sub-maxima came together with

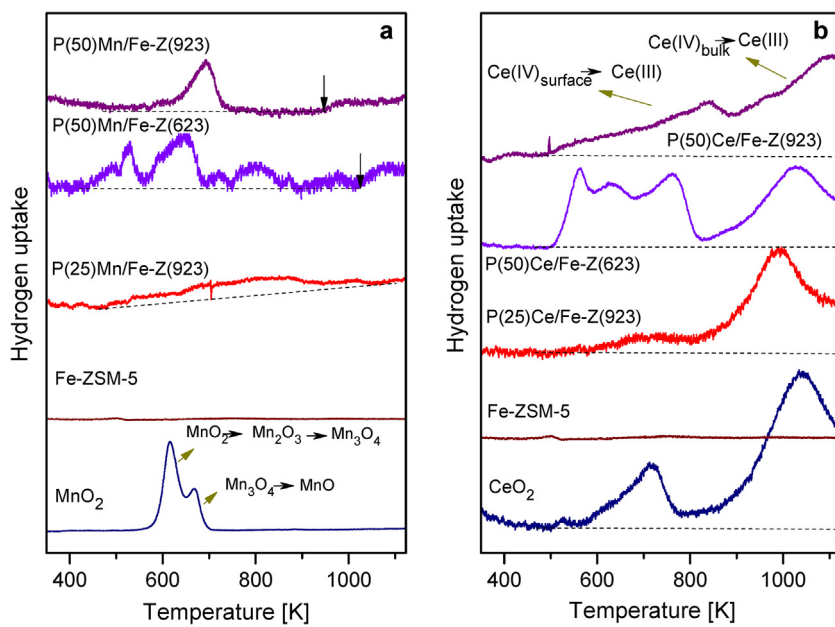


Fig. 3. TPR profiles of precipitated hybrid catalysts after calcination at 623 K or 923 K and of reference compounds.

a strongly attenuated high-temperature peak. This indicates a very high dispersion of the ceria phase on the zeolite crystal. After calcination at 923 K, the high-temperature peak became predominant in both samples. Notably, in P(50)Ce/Fe-Z(923), reduction started at almost the same temperature as after low-temperature calcination (P(50)Ce/Fe-Z(623)). This suggests that the sample still contained significant amounts of highly disperse material, unlike P(25)Ce/Fe-Z(923) where intensity in the low-temperature region is very small. The reason for this difference is unknown. In these samples, observation of the signal in the isothermal phase at 1123 K (not shown) proved ongoing reduction. The exact course of the baseline was therefore difficult to establish. Table 2 gives reduction degrees evaluated without baseline correction. They are slightly below 50%, without obvious tendencies.

3.2. Catalysis

In Fig. 4, NO and NH₃ conversions over Mn₂O₃/Fe-ZSM-5 composites made by mechanical mixing and by precipitation are compared. Negative conversions as observed with the pure Mn oxide at higher temperatures have not been depicted. The physical mixture exhibited high NO conversions at low temperatures as reported in our previous paper [9], but the performance reported there could not be completely reproduced. While the light-off temperature T_{50} (temperature of 50% conversion) was increased by almost 50 K in the present study, the temperature range of selective NO conversion was much broader. This is probably due to the more crystalline nature of the Mn₃O₄ employed now (Fig. 1a): the oxide used in [9] was a mixture of disordered phases (carbonate, hydroxide, oxide). While the expectation that the precipitates might outperform the mixture was not fulfilled, the sample with the lower Mn content (P(25)Mn/Fe-Z(623)) provided higher peak NO conversion and a broader temperature range of selective conversion at only slightly increased light-off temperature (Fig. 4a). This is probably due to a lower oxidation activity of the Mn component towards NH₃. Indeed, an only slightly increased Mn content of P(50)Mn/Fe-Z(623) (cf. Table 1) resulted in a less favorable catalytic behavior.

Fig. 4b reports the effect of high-temperature calcination on the catalytic properties. As anticipated from results shown in [9],

a strong synergy was still observed with the mechanical mixture although performance was significantly affected and the catalyst was outperformed by a mixture of separately calcined MnO_x with Fe-ZSM-5, which is shown in Fig. 4b for comparison. Adverse effects of high-temperature calcination were, however, much stronger with the precipitated hybrids. The more active one (P(25)Mn/Fe-Z(623)) did not even achieve the NO conversions of the zeolite component at any temperature: the manganese had simply turned into a poison after the treatment. It should be noted that this is not a selectivity problem because NH₃ conversions equaled NO conversions up to 673 K (with P(50)Mn/Fe-Z up to 573 K). Both conversions grew more sluggish with temperature than after low-temperature calcination, i.e., there is a significant drop in the apparent activation energy for both catalysts. Apparent activation energies E_A for the temperature range up to 600 K were estimated assuming a first-order reaction kinetics for standard SCR. For P(50)Mn/Fe-Z, E_A decreased from 36 to 29.5 kJ/mol, for P(25)Mn/Fe-Z from 42 to 20.5 kJ/mol.

Mn-based catalysts are known to release by-products (N₂O, NO₂) during NH₃-SCR, and we have shown in earlier work that this tendency is suppressed but not removed in the hybrid catalysts [9]. The same trends can be seen with the precipitated hybrids (Fig. S-1, supplementary information). This holds both for N₂O and NO₂ release, which is much weaker over the hybrids than over the pure manganese oxides. Calcination at 923 K further suppressed formation of both N₂O and NO₂.

Reaction data for the CeO₂-Fe-ZSM-5 system are shown in Fig. 5. These catalysts did not produce N₂O to any detectable extent while minor NO₂ formation was seen above 770 K (not shown). As expected, activities obtained with this system were smaller than with the Mn-based composites, but synergies were clearly observed. Precipitates of CeO₂ onto Fe-ZSM-5 were significantly more active than the physical mixture, for which a synergy could be identified only at above 700 K (Fig. 5a). Differences between the behavior of catalysts with different CeO₂ contents after low-temperature calcination seem to be minor, but the higher low-temperature conversions observed with P(25)Ce/Fe-Z resulted in a somewhat smaller activation energy over this catalyst (49 kJ/mol, P(50)Ce/Fe-Z: 61.5 kJ/mol, for temperatures up to 600 K). After high-temperature calcination, deactivation was again

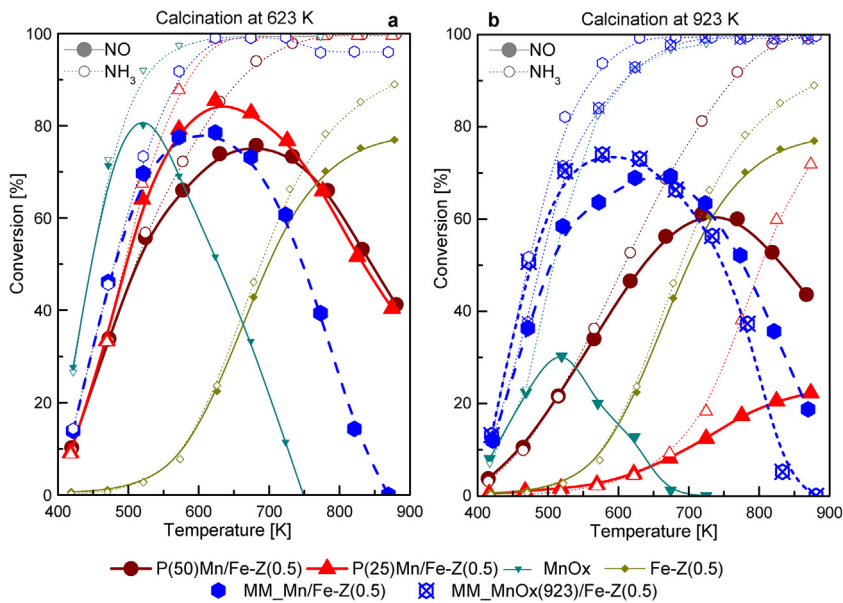


Fig. 4. NO and NH₃ conversion curves of hybrids based on MnOx and Fe-ZSM-5 and of pure compounds; physically mixed hybrids (MM) compared with precipitates (P), a, after calcination at 623 K, b, after calcination at 923 K, performance of a physical mixture of MnOx calcined at 923 K and Fe-ZSM-5 given for comparison. 1000 ppm NO, 1000 ppm NH₃, 2% O₂ in He, at 300,000 h⁻¹ (hybrids) or 600,00 h⁻¹ (pure components). Apparent activation energies estimated for T ≤ 523 K from panel a, for T ≤ 573 K from panel b: P(25)Mn/Fe-Z after calcination at 623 K – 42 kJ/mol, at 923 K – 20.5 kJ/mol, P(50)Mn/Fe-Z after calcination at 623 K – 36 kJ/mol, at 923 K – 29.5 kJ/mol.

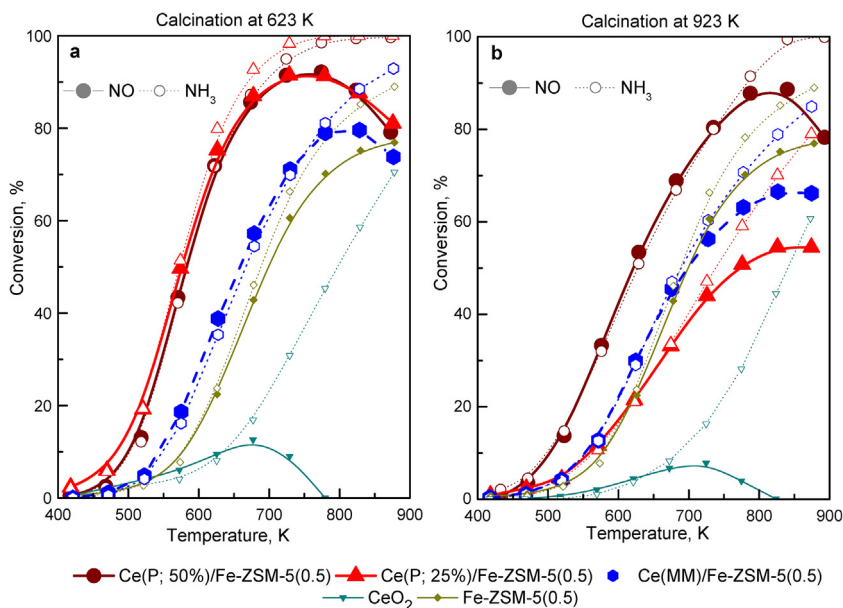


Fig. 5. NO and NH₃ conversion curves of hybrids based on CeO₂ and Fe-ZSM-5 and of pure compounds; physically mixed hybrids (MM) compared with precipitates (P), a, after calcination at 623 K, b, after calcination at 923 K. For experimental conditions see Fig. 4. Apparent activation energies estimated for T ≤ 573 K: P(25)Ce/Fe-Z after calcination at 623 K – 49 kJ/mol, at 923 K – 38 kJ/mol, P(50)Ce/Fe-Z after calcination at 623 K – 61.5 kJ/mol, at 923 K – 48 kJ/mol.

more drastic with the catalyst containing less precipitated material (Fig. 5b). While the light-off temperature of P(50)Ce/Fe-Z was shifted by just about 40 K, P(25)Ce/Fe-Z turned out to be inferior even to the Fe-ZSM-5 in it at most temperatures. Again, there was a drop in the apparent activation energies upon high-temperature calcination but less dramatic than in case of the MnOx/Fe-ZSM-5 system: E_A was estimated to 38 kJ/mol for P(25)Ce/Fe-Z, and 48 kJ/mol for P(50)Ce/Fe-Z. NO conversions over the physical mixture were close to those of the pure Fe-ZSM-5 except for the highest temperatures.

Precipitates with CeZrO_x were studied for several reasons. The well-known higher oxygen mobility in the mixed oxide should improve its oxidation activity relatively to CeO₂, and a higher sta-

bility towards sintering might prevent the drastic deactivation phenomena observed with the binary oxide. CeZrO_x-based composites were made both with Fe-ZSM-5 and with H-ZSM-5, because it has been found recently that the presence of a redox cation in the zeolite is not required to obtain the synergistic effect [6,7].

Fig. 6 summarizes the behavior of composites containing CeZrO_x and H-ZSM-5. The synergistic effect is very drastic here because neither H-ZSM-5 nor CeZrO_x are good standard SCR catalysts. Again, precipitated hybrids were more active than the physical mixture (Fig. 6a), but the difference was smaller than with the hybrids made of CeO₂ and Fe-ZSM-5. After both thermal treatments, the precipitate with the higher mixed-oxide content was somewhat more active. There was indeed a stabilizing impact of zirconium

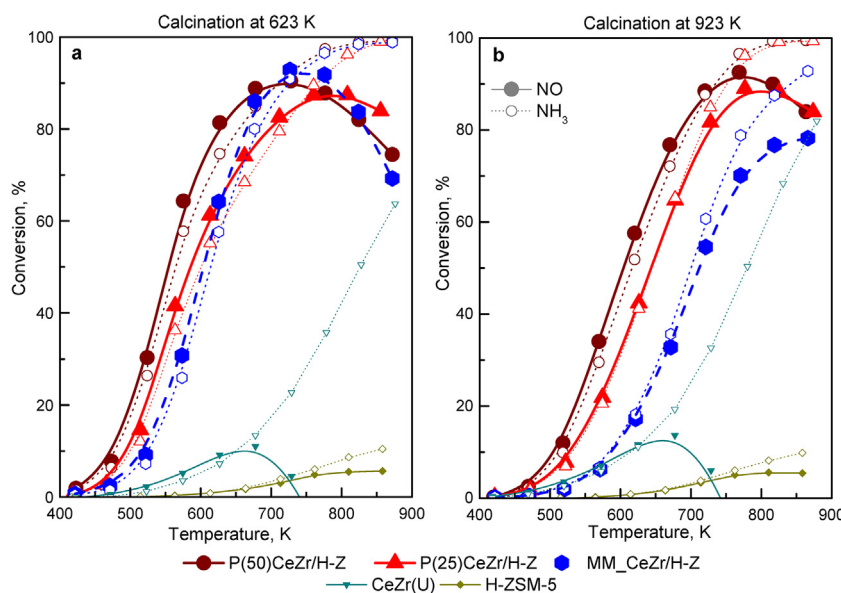


Fig. 6. NO and NH₃ conversion curves of hybrids based on CeZrOx and H-ZSM-5 and of pure compounds; physically mixed hybrids (MM) compared with precipitates (P), a, after calcination at 623 K, b, after calcination at 923 K. For experimental conditions see Fig. 4. Apparent activation energies estimated for T \leq 573 K: P(25)CeZr/H-Z after calcination at 623 K – 57 kJ/mol, at 923 K – 55 kJ/mol, P(50)CeZr/H-Z after calcination at 623 K – 53.5 kJ/mol, at 923 K – 56.5 kJ/mol.

in these catalysts: with both samples, the light-off temperature was increased by 50–60 K after treatment at 923 K, which is much smaller than the 200 K shift suffered by P(25)Ce/Fe-Z (Fig. 5). Moreover, no change in activation energies could be detected in these catalysts after high-temperature calcination (see legend of Fig. 6). Surprisingly, the deactivation of the physical mixture of CeZrOx and H-ZSM-5 was even more severe than that of the precipitates, its T₅₀ increased by more than 100 K (to 715 K, Fig. 6), which also exceeds the 40 K shift observed for the physical mixture without Zr (MM(50)Ce/Fe-Z, cf. Fig. 5).

Activities measured with composites made of CeZrOx and Fe-ZSM-5 are summarized in Fig. 7 where mixture and precipitate with (intended) 50% CeZrOx are compared. Activities of the precipitates on Fe-ZSM-5 and H-ZSM-5 are similar (T₅₀ = 565 K and 555 K, respectively, Figs. 6 and 7), both are slightly more active than the Zr-free precipitate (Fig. 5a, T₅₀ = 582 K). At higher temperatures, however, both NO and NH₃ conversions grew more sluggish with the Fe-ZSM-5 based sample for unknown reasons (Fig. 7). Due to this effect, one may suppose a decrease of activation energies by mere optical inspection, however, below 600 K, there was indeed no change (see legend to Fig. 7). Notably, the physical mixture of CeZrOx and Fe-ZSM-5 performed best among the three Ce-based physical mixtures studied (cf.), with a light-off temperature of 575 K and full NO conversion in a certain, though narrow temperature range. This was not achieved by any other catalyst studied here. After calcination at 923 K, however, this catalyst suffered deactivation as well.

4. Discussion

The goal of the present study is to assess the catalytic behavior of precipitate hybrids in standard SCR, and to compare it with that of mechanical mixtures. In judging on catalyst behavior, attention will be focused on activity and stability. Regarding activity, we found that precipitated hybrids usually outperform physically mixed systems, with an exception in the case of Mn-based catalysts. Regarding stability, rather diverse tendencies were observed: while some MnO_x- and CeO₂-based catalysts suffered unexpectedly drastic deactivation by thermal stress (Figs. 4 and 5), precipitates based

on CeZrOx could be even more stable than the related mechanical mixtures (Fig. 6).

In the following, we will discuss these observations in the light of our characterization data and of what we know about the catalytic mechanism operating in these hybrids. While some trends will become plausible on this basis, not all phenomena will find satisfactory explanation because interpretation of the characterization data of these complex systems is not always unambiguous and the catalytic mechanism is not yet fully established.

According to our previous work, this mechanism includes a transport step in which an unstable intermediate leaves a site of the oxide component and finds a site in the “SCR” component, most likely a zeolite proton. Activation energies far above those of diffusion steps tell that the transport step is not rate determining – but it is necessary. While sites of oxidation component and zeolite are clearly separate in the physical mixture with the exception of the direct contact points between components, the average distance becomes much smaller in the precipitate. At the same time, the identity of the oxidation component may be strongly modified by interaction with the zeolite surface in this case. Direct interaction of the cations with zeolite protons (exchange, probably with retention of extra-lattice oxygen) may drastically modify their redox behavior and catalytic properties. Such exchanged cations will not be available for the formation of a bulk oxide phase, which is most relevant for preparations with low oxide contents.

Upon thermal stress, chemical transformations and sintering of oxide particles will proceed different in lose or intense interaction with the zeolite. Sintering in physical mixtures is difficult to predict because it depends on the contacts between oxide particles and zeolite, which may cause competing interactions. In our previous work [9], no clear influence of the zeolite was detected when comparing sintering of Mn-Ce and Mn-Cu mixed oxides in presence or absence of the zeolite component. Interactions with the zeolite surface should generally interfere with sintering by offering SSIE as an additional reaction route. The result of this competition should depend on the cohesion of the oxide particles, which can be inferred from their thermal stability (e.g. CeZrOx > CeO₂). The SSIE route may be more favorable for Mn(III) species which might migrate as MnO⁺ entities than for Ce species which tend to be tetravalent under our calcination conditions. In physical mixtures, SSIE will be initially

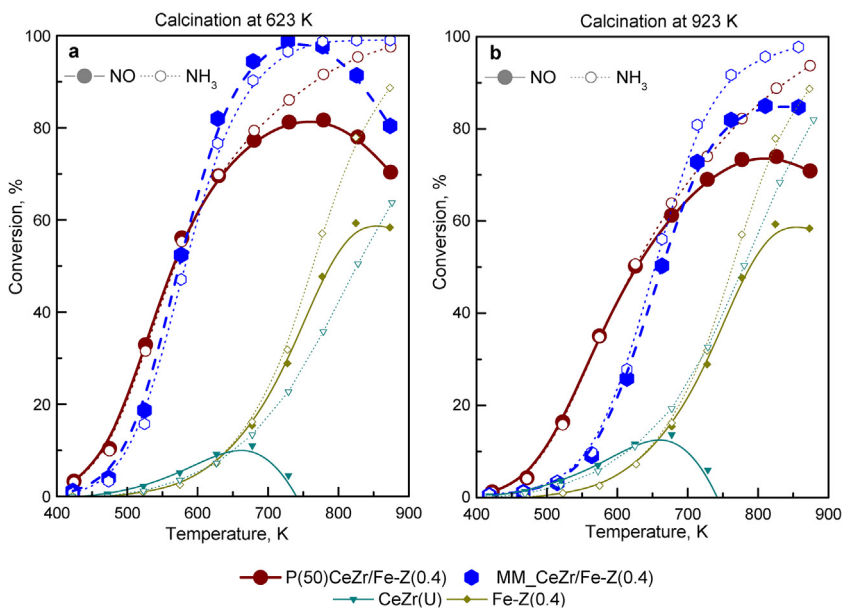


Fig. 7. NO and NH₃ conversion curves of hybrids based on CeZrOx and Fe-ZSM-5 and of pure compounds; physically mixed hybrid (MM) compared with precipitate (P), a, after calcination at 623 K, b, after calcination at 923 K. For experimental conditions see Fig. 4. Apparent activation energies estimated for T \leq 573 K: P(50)CeZr/Fe-Z after calcination at 623 K – 43.5 kJ/mol, at 923 K – 45 kJ/mol.

confined to the contact points between oxide and zeolite, but it may take up pace when the exchange proceeds across the surface as a route of surface diffusion. In precipitates, the whole surface is likely to be largely exchanged by the redox cation during preparation, therefore SSIE should be much more intense. Here, surface diffusion would proceed largely across surface already exchanged with the cation. The influence of these differences on transport rates is difficult to predict. We have not studied this aspect systematically, but obviously sintering is severe also in precipitated systems as can be seen in Fig. 1b and in particular in Fig. 2 where line widths after high-temperature calcination are not very different for the pure and the precipitated versions of the CeZrOx redox component.

Changes of BET surface area upon precipitation and subsequent thermal treatment (Table 1) comprise contributions from pore plugging in the zeolite support and from the additional surface provided by the precipitate. Pore plugging should not be primarily related to solid-state ion exchange because the migrating species are most likely very small. It will rather occur upon aggregation of oligomeric oxide entities, where SSIE may contribute additional material.

Precipitation with low-temperature calcination did either not affect BET surface areas significantly (Mn-based precipitates, with low oxide content; CeZrOx on H-ZSM-5) or decreased it, sometimes drastically. Notably, the BET surface area was more affected in precipitates on Fe-ZSM-5 than on H-ZSM-5, in particular in the Ce-only catalysts, where particles are apparently larger (cf. Figs. 1 and 2). The latter is somewhat unexpected because a few large particles should be less effective in pore plugging than many small particles, but such correlation is misleading because pore entrances could well be blocked by very small disordered clusters invisible in XRD.

After calcination at 923 K, both TPR (Fig. 3, Table 2) and nitrogen physisorption (Table 1) indicate that Mn underwent solid-state ion exchange to a much larger extent in P(25)Mn/Fe-Z than in P(50)Mn/Fe-Z despite the rather similar actual Mn contents (Table 1). The reason for this difference is not clear, but the absence of a clear low-temperature TPR signal in P(25)Mn/Fe-Z, but not in P(50)Mn/Fe-Z, as well as the lower reducibility of Mn in the former sample and the pronounced loss in BET surface area indicate a larger mobility of Mn in this sample.

After low-temperature calcination, the P(50)Ce/Fe-Z sample exhibited a much more intense and complex low-temperature TPR signal than CeO₂ (Fig. 3), which illustrates the strong influence of the zeolite surface on the oxide, which is just “CeO₂” according to XRD. In the Ce-containing precipitates, the particle size did not correlate with the BET surface area (Table 1): the CeZrOx precipitates with their smaller particles (broader XRD signals) have the higher BET surface areas, which may be related to a better cohesion already of smaller particles and therefore less pore blocking by disperse material. In these composites pore blocking became a problem only after thermal stress. The latter shows that interaction with the zeolite causes mobility also in Ce-based systems. However, BET surface areas of the mixed-oxide based hybrids remained clearly above that achieved with P(50)Ce/Fe-Z(923), and at the lower mixed-oxide content, pore plugging (or the net effect of pore plugging and oxide sintering) was even negligible. It is also notable that the precipitate on Fe-ZSM-5 exhibited a rather low BET surface area already after low-temperature calcination, in line with the almost identical value of P(25)Ce/Fe-ZSM-5 with a similar oxide content (31.7% vs. 34.7%).

The superiority of the precipitates over the physical mixtures in catalysis may arise from the closer proximity of redox and acidic sites or from higher redox activity of the more disordered surface of the oxidation component. As these influences cannot be varied separately it is difficult to differentiate between them. However, the observation that high-temperature calcination leaves P(50)Ce/Fe-Z more active than even the physical mixture calcined at only 623 K (cf. Fig. 5; in Fig. 6, P(50)CeZr/H-Z(923) and MM.CeZr/H-ZSM-5 exhibit approximately identical light-off temperatures) suggests that the distance plays an important role as well. On the other hand, there is no clear correlation between BET surface area, which indicates the accessibility of the zeolite interior, and activity. Samples with low BET surface area often exhibit poor performance though. However, the loss in activity of P(25)Mn/Fe-Z(923) as compared to its P(50) counterpart or even to Fe-ZSM-5 (Fig. 4b) is much stronger than the 30% loss in BET surface area (Table 1). After high-temperature calcination of the CeO₂-based precipitates, the catalyst with the lowest BET surface area (P(50)Ce/Fe-Z) showed the best performance (Fig. 5b). The relation between activities of H-

ZSM-5-supported CeZrOx was not changed by the thermal stress: the ratio of rate constants at 523 K between P(50)CeZr/H-Z and P(25)CeZr/H-Z was 1.9 after calcination at 923 K, and 1.8 after calcination at 623 K although the former lost 25% of its BET surface area by the severe treatment as compared to 2.5% for the latter. This suggests that only a minor part of the zeolite sites was involved in the reaction.

Deactivation is the most serious problem with the composites, and we found rather drastic examples for it (Figs. 5 b, 6 b). Deactivation may be caused by stabilization (and therefore smaller redox activity) of the redox component and by poisoning of the zeolite protons. The former has been examined by measuring conversions in NO oxidation for P(25)Mn/Fe-Z after calcination at 623 K or at 923 K (Fig. S-2). The difference is dramatic. It is known that Mn cations on exchange positions provide very low activity in NO oxidation [18], therefore, the loss of activity confirms our conclusion on solid-state ion exchange proceeding in this sample at elevated temperature. On the other hand, the increase in NO conversion over P(25)Mn/Fe-Z(923) by an order of magnitude in a 100 K temperature interval between 550 and 650 K is not reflected in its standard SCR conversion curve (Fig. 4b). The activation energy of standard SCR decreased upon calcination unlike the activation energy in NO oxidation. Therefore, although NO oxidation is probably part of the reaction mechanism being the source of intermediates, other effects appear to contribute to the observed deactivation as well.

In our particular mechanism, an increase of the distance between oxidation component and protons (e.g. by poisoning of adjacent protons via SSIE) should also be envisaged. In this context, it may be relevant that deactivation was often accompanied by a decrease of the apparent activation energy. High activity is frequently related to low activation energy and high abundance of active sites. Simultaneous loss of activity and activation energy as observed here may be caused by a transport step becoming influential in the reaction kinetics. This would not be film diffusion or pore diffusion because conditions were not changed in the comparative experiments (for a general discussion of transport steps in our experiments see [19]), but it may be the transport step between the redox oxide and the nearest Brønsted sites. As mentioned above, this might happen by solid-state ion exchange of the redox cation if the latter becomes deactivated for the SCR reaction at the exchange position. The stronger effect observed with Mn catalysts would agree with this view because of the expected higher mobility of Mn oxo ions. We did not check NO oxidation activity of Mn-exchanged zeolites, but their standard SCR activity [20]. The latter was negligible as long as the presence of extra-zeolite Mn oxide species was avoided. The particular susceptibility of the Mn-based precipitates to deactivation may also explain why this system was the only one in which the precipitate route did not provide superior SCR activity.

The extent of deactivation observed in some cases deserves some additional comment, because the hybrids P(25)Mn/Fe-Z(923), but also P(25)Ce/Fe-Z (cf. Figs. 4 b, 5 b) ended up with activities below that of the zeolite component in them, although the latter should be expected to contribute its own activity even when the other component has been destroyed. The effect is not due to pore blockage: in P(25)Mn/Fe-Z(923), 70% of the pore system were still accessible (Table 1) while the loss in reaction rate is 1–2 orders of magnitude and the low activation energy suggests that the rate-determining step does not proceed on a Fe site under these conditions. The poisoning of the Fe sites may be ascribed to the removal of nearby Brønsted sites by dry exchange (SSIE) with MnO⁺, provided such sites are required in the reaction mechanism, or by direct interaction between mobile Mn species and Fe sites.

Discussion on the role of Brønsted sites in standard SCR over Fe zeolites is not yet settled [21–24]. According to a popular proposal, standard SCR proceeds as a sequence of NO₂ formation and fast SCR [21,25], the latter step being catalyzed by Brønsted sites. These

ideas have been, however, criticized for various reasons [19,26–29]. Most significantly, fast SCR over an unmodified H-ZSM-5 not containing Fe impurities has been found to be way too slow to explain standard SCR rates usually observed [29]. Brønsted acidity was reported to favor standard SCR over Fe zeolites not being, however, a prerequisite for its occurrence [30,31]. Recent mechanistic proposals for standard SCR over redox zeolites [32,33] indeed do without Brønsted sites. Therefore, poisoning of the Brønsted sites by SSIE by migrating Mn species should not remove the contribution of Fe sites to activity.

On the other hand, an alternative mechanism for standard SCR has been recently demonstrated, in which a *stable* volatile intermediate with N in (average) +3 oxidation state (N₂O₃, HONO mentioned as candidates) is formed over Fe sites and decomposed over zeolite protons [34]. In our hybrid systems, the crucial role of Brønsted acidity has been demonstrated by poisoning experiments, in which replacement of H-ZSM-5 by Na-ZSM-5 quenched SCR activity of the hybrid completely [35] while residual activity was left when Na was deposited on the oxidation component [36]. The situation suggests strongly that standard SCR may proceed via different routes depending on catalyst configurations offered. There are obviously two different bifunctional mechanisms, either via a stable [34] or via an unstable intermediate [8], and we do not mean to reject alternative mechanisms proceeding on individual sites by this although the role of the various routes will have to be elucidated for each situation.

As to deactivation, the option that mobile MnO_x species interact directly with Fe sites (isolated Fe oxo sites or oligomeric clusters of low nuclearity [29,37,38]) leaving them deactivated should also be considered. Due to the low Fe content, complete poisoning of the Fe sites by the limited quantity of Mn species available would probably require some preference in the interaction between the transition-metal oxide species over interaction with nearby protons. Our BET studies contain some features suggesting that there is such preference in the interaction with Ce oxo species. Normally, one would not expect the low amount of Fe present in the external surface of 0.4 or 0.5 wt-% Fe-ZSM-5 to exert an influence on the precipitation process of CeO₂ or CeZrOx. However, such influence is just what we obtained: Precipitation of 37 wt-% CeZrOx onto H-ZSM-5 did not cause significant pore plugging (Table 1, P(50)CeZr/H-Z(623)), which was, however, significant after depositing 35 wt-% CeZrOx or only 32 wt-% CeO₂ on Fe-ZSM-5 (P(50)CeZr/Fe-Z(623), P(25)Ce/Fe-Z(623)). It seems, therefore, that interactions with Fe oxo surface sites may have attracted Ce(Zr)Ox entities resulting in clustering and pore plugging already after mild calcination.

5. Conclusions

Precipitation of an oxidation catalyst on an acidic zeolite is an alternative route to hybrid catalysts for the selective catalytic reduction of NO by NH₃, which were originally introduced as physical mixtures between the components. For CeO₂ and CeZrOx combined with Fe-ZSM-5 and H-ZSM-5, precipitated hybrids were more active than physically mixed hybrids. A reversed ranking in the case of the MnO_x/Fe-ZSM-5 system may be due to a particular susceptibility of the corresponding precipitates to deactivation. Precipitated hybrids are very prone to thermal deactivation, which was ascribed to an increased opportunity for the redox oxides to undergo solid-state ion exchange when deposited onto the zeolite crystals. If drastic, this deactivation is accompanied by a significant decrease of the apparent activation energy of NH₃-SCR. This may support earlier conclusions according to which the reaction mechanism operating in the hybrids comprises a transport step of an unstable intermediate, which might become rate limiting when

acidic sites in the vicinity of the oxidation sites have become poisoned by solid-state ion exchange.

Acknowledgements

We gratefully acknowledge Dr. S. Kaluza and Mr. W. Ludwig from Fraunhofer Institute for Environmental, Safety, and Energy Technology UMSICHT Oberhausen, Germany, for elemental analyses, Dr. Th. Reinicke (Ruhr University Bochum) for XRD measurements and Ms. N. Arshadi (Ruhr University Bochum) for physisorption analyses.

Appendix A. Supplementary data

Supplementary data associated with this article can be found, in the online version, at <http://dx.doi.org/10.1016/j.apcatb.2017.06.079>.

References

- [1] Urea-SCR Technology for deNO_x After Treatment of Diesel Exhausts, in: I. Nova, E. Tronconi (Eds.), Springer, Berlin-Heidelberg-New York, 2014.
- [2] J. Li, H. Chang, L. Ma, J. Hao, R.T. Yang, *Catal. Today* 175 (2011) 147–156.
- [3] A.Y. Stakheev, G.N. Baeva, G.O. Bragina, N.S. Teleguina, A.L. Kustov, M. Grill, J.R. Thogersen, *Top. Catal.* 56 (2013) 427–433.
- [4] A.Y. Stakheev, A.I. Mytareva, D.A. Bokarev, G.N. Baeva, D.S. Krivoruchenko, A.L. Kustov, M. Grill, J.R. Thogersen, *Catal. Today* 258 (2015) 183–189.
- [5] A.I. Mytareva, D.A. Bokarev, G.N. Baeva, D.S. Krivoruchenko, A.Y. Belyankin, A.Y. Stakheev, *Petr. Chem.* 56 (2016) 211–216.
- [6] A.I. Mytareva, A.Y. Stakheev, G.N. Baeva, D.A. Bokarev, A.L. Kustov, J.R. Thogersen, *Top. Catal.* 59 (2016) 919–924.
- [7] M. Salazar, S. Hoffmann, V. Singer, R. Becker, W. Grünert, *Appl. Catal. B* 199 (2016) 433–438.
- [8] M. Salazar, S. Hoffmann, O.P. Tkachenko, R. Becker, W. Grünert, *Appl. Catal. B* 182 (2016) 213–219.
- [9] M. Salazar, R. Becker, W. Grünert, *Appl. Catal. B* 165 (2015) 316–327.
- [10] T. Liese, E. Löffler, W. Grünert, *J. Catal.* 197 (2001) 123–130.
- [11] T. Liese, D. Rutenbeck, W. Grünert, 12th International Zeolite Conference, in: M.M.J. Treacy, B.K. Marcus, M.E. Bisher, J.B. Higgins (Eds.), Materials Research Society, Baltimore (USA), 1998, pp. 2795–2802.
- [12] C. Yokoyama, M. Misono, *Catal. Today* 22 (1994) 59–72.
- [13] M. Schwidder, S. Heikens, A. De Toni, S. Geisler, M. Berndt, A. Brückner, W. Grünert, *J. Catal.* 259 (2008) 96–103.
- [14] B.R. Strohmeier, D.M. Hercules, *J. Phys. Chem.* 88 (1984) 4922–4929.
- [15] E.R. Stobbe, B.A. de Boer, J.W. Geus, *Catal. Today* 47 (1999) 161–167.
- [16] A. Trovarelli, *Catal. Rev. Sci. Eng.* 38 (1996) 439–520.
- [17] F. Giordano, A. Trovarelli, C. de Leitenburg, M. Giona, *J. Catal.* 193 (2000) 273–282.
- [18] D.S. Krivoruchenko, A.V. Kucherov, N.S. Teleguina, D.A. Bokarev, P. Selvam, A.Y. Stakheev, *Russ. Chem. Bull.* 63 (2014) 389–395.
- [19] I. Ellmers, R.P. Vélez, U. Bentrup, A. Brückner, W. Grünert, *J. Catal.* 311 (2014) 199–211.
- [20] L. Tillmann, B. Sc. Thesis, Bochum, Ruhr University, 2013.
- [21] S. Brandenberger, O. Kröcher, A. Tissler, R. Althoff, *Catal. Rev. Sci. Eng.* 50 (2008) 492–531.
- [22] W. Grünert, Urea-SCR Technology for deNO_x After Treatment of Diesel Exhausts, in: I. Nova, E. Tronconi (Eds.), Springer, Berlin-Heidelberg-New York, 2014, pp. 181–220.
- [23] M. Iwasaki, Urea-SCR Technology for deNO_x After Treatment of Diesel Exhausts, in: I. Nova, E. Tronconi (Eds.), Springer, Berlin-Heidelberg-New York, 2014, pp. 221–246.
- [24] E. Tronconi, I. Nova, Urea-SCR Technology for deNO_x After Treatment of Diesel Exhausts, in: I. Nova, E. Tronconi (Eds.), Springer, Berlin-Heidelberg-New York, 2014, pp. 247–272.
- [25] R.Q. Long, R.T. Yang, *J. Catal.* 207 (2002) 224–231.
- [26] M. Ruggeri, I. Nova, E. Tronconi, *Top. Catal.* 56 (2013) 109–113.
- [27] M.P. Ruggeri, T. Selleri, M. Colombo, I. Nova, E. Tronconi, *J. Catal.* 311 (2014) 266–270.
- [28] M.P. Ruggeri, T. Selleri, M. Colombo, I. Nova, E. Tronconi, *J. Catal.* 328 (2015) 258–269.
- [29] I. Ellmers, R. Pérez Vélez, U. Bentrup, W. Schwieger, A. Brückner, W. Grünert, *Catal. Today* 258 (2015) 337–346.
- [30] M. Schwidder, M. Santhosh Kumar, U. Bentrup, J. Perez-Ramirez, A. Brückner, W. Grünert, *Microporous Mesoporous Mat.* 111 (2008) 124–133.
- [31] S. Brandenberger, O. Kröcher, A. Wokaun, A. Tissler, R. Althoff, *J. Catal.* 268 (2010) 297–306.
- [32] T.V.W. Janssens, H. Falsig, L.F. Lundsgaard, P.N.R. Venneström, S.B. Rasmussen, P.G. Moses, F. Giordanino, E. Borfecchia, K.A. Lomachenko, C. Lamberti, S. Bordiga, A. Godiksen, S. Mossin, P. Beato, *ACS Catal.* 5 (2015) 2832–2845.
- [33] D.E. Doronkin, M. Casapu, T. Günter, O. Müller, R. Frahm, J.D. Grunwaldt, *J. Phys. Chem. C* 118 (2014) 10204–10212.
- [34] T. Selleri, I. Nova, E. Tronconi, *Appl. Catal. B* 206 (2017) 471–478.
- [35] S. Hoffmann, M. Sc. Thesis, Bochum, 2015.
- [36] P.S. Joshi, W. Grünert, to be published.
- [37] M. Schwidder, M. Santhosh Kumar, K.V. Klementiev, M.M. Pohl, A. Brückner, W. Grünert, *J. Catal.* 231 (2005) 314–330.
- [38] S. Brandenberger, O. Kröcher, A. Tissler, R. Althoff, *Appl. Catal. B* 95 (2010) 348–357.